Hierarchic Structure of Shish-Kebab by Neutron Scattering in a Wide *Q* Range

Toshiji Kanaya,* Go Matsuba, Yoshiko Ogino, and Koji Nishida

Institute for Chemical Research, Kyoto University, Uji, Kyoto-fu 611-0011, Japan

Hirohiko M. Shimizu and Takenao Shinohara

RIKEN, 2-1 Hirosawa, Wako, Saitama-ken 351-0198, Japan

Takayuki Oku and Junichi Suzuki

Quantum Beam Science Directorate, Japan Atomic Energy Agency (JAEA), 2-4 Shirakata-Shirane, Tokai, Ibaraki-ken, 319-1195, Japan

Toshiya Otomo

Neutron Science Laboratory, High Energy Accelerator Research Organization (KEK), 1-1 Oho, Tsukuba, Ibaraki-ken 305-0801, Japan

Received November 12, 2006; Revised Manuscript Received March 3, 2007

ABSTRACT: We performed small-angle neutron and X-ray scattering (SANS and SAXS) measurements on an elongated blend of low molecular weight deuterated polyethylene (PE) and high molecular weight hydrogenated one (97.2/2.8) in a very wide range of scattering vector of 1×10^{-4}−3 Å^{-1} to elucidate hierarchic structure of the so-called shish-kebab. Comparing the SANS and SAXS data, we found that the hydrogenated high molecular weight PE formed a large and long object aligned along the elongation direction. The SANS data were analyzed in terms of the multicore−shell cylinder model, and we found that the long oriented structure had radius of ∼1 μm and length of ∼12 μm and included about three extended chain crystals with radius of ∼45 Å. We believe that this oriented long object with a relatively low aspect ratio of about 12:1, which is called the row structure in this paper, is a precursor formed from deformation of network of high molecular weight components due to entanglements.

1. Introduction

Polymer materials are crystallized under many kinds of flows during their processing such as fiber spinning, injection molding, and extrusion, and the crystallization kinetics and the final morphology dominate their macroscopic properties. In flow crystallization processes the so-called shish-kebab structure is often observed in the morphology, which consists of a long central core (shish) surrounded by lamellar crystals (kebabs). It is believed that the shish-kebab structure is the origin of the ultrahigh strength and modulus of fibers, so extensive studies have been performed to elucidate the morphology and the processes of formation.[1−17] Such shish-kebab structure in polyethylene (PE) was observed by Keller et al. using transmission electron microscope (TEM),[18−21] showing shish of ∼100 Å in diameter and several micrometers in length. It is believed that the shish is an extended chain crystal and the kebab is a folded chain lamella crystal. On the other hand, long oriented objects with diameters of several micrometers aligned along the flow direction are often observed in some polymers[8,22] using an optical microscope (OM). This long object is apparently similar to the shish structure, which is called the row structure in this paper, but the spatial scale is very different. It may include the kebab inside judging from the spatial scale. These observations suggest that the shish-kebab has hierarchic structure in a wide spatial scale. However, few works dealt with the hierarchic structure of the shish-kebab. One of the reasons is difficulty to study the shish-kebab structure in a wide spatial range simultaneously; in addition, the kebabs are overlapped on the shish, so that it is not easy to distinguish the shish from the kebabs.

In a previous paper,[17] we performed depolarized light scattering (DPLS) experiments on a blend of low molecular weight PE (LMW PE) and a small amount of ultrahigh molecular weight PE (HMW PE) to study effects of the high molecular weight component on shish-kebab formation and found that HMW PE enhanced the formation of shish-kebab above a certain critical concentration, which was about 3 times larger than the overlap concentration. Furthermore, we studied an elongated PE blend of deuterated low molecular weight PE (LMW-d-PE, 97.2 wt %) and hydrogenated HMW PE (HMW-h-PE, 2.8 wt %) by small-angle neutron and small-angle X-ray scattering (SANS and SAXS) to confirm that the shishlike structure is formed from the HMW component. The results are reproduced in Figure 1.

In the SANS data in Figure 1a we clearly see the streaklike scattering normal to the elongation direction in addition to the two-spot pattern along the elongation direction. The former and the latter correspond to the shishlike structure (or the row structure) and the kebab structure (or the kebab spacing). On the other hand, we only see the two-spot pattern along the elongation direction in the SAXS result (Figure 1b), corresponding to the kebab structure. This result directly tells us that the shishlike structure or the row structure is formed from the HMW component. Conventional SANS machines can access a *Q* range down to ∼3×10^{-3} Å^{-1}, corresponding to ∼2000 Å in real space, which is not enough to see the row structure on

* Corresponding author: Tel +81-774-38-3141; Fax +81-774-38-3146; e-mail kanaya@scl.kyoto-u.ac.jp.

10.1021/ma062606z CCC: $37.00
Published on Web 04/14/2007

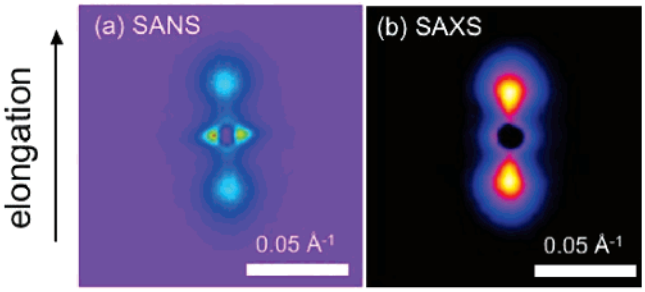

Figure 1. 2D SANS (a) and SAXS (b) patterns of elongated PE blend of low molecular weight deuterated PE (LMW-d-PE) with M_w = 200 000 and high molecular weight hydrogenated PE (HMW-h-PE) with molecular weight M_w = 2 000 000. Weight fraction of HMW-h-PE is 2.8%.

the micrometer scale. In this work we therefore performed SANS measurements with a machine equipped with neutron lenses to access a very low Q range down to $\sim 1 \times 10^{-4}$ Å^{-1}. In addition, we performed SANS measurements using a time-of-flight (TOF) SANS machine on a spallation cold neutron source to cover a Q range from 10^{-2} to 3 Å^{-1}. This measurement gives us information on crystal lattice, too. In this paper we will analyze the data in the wide Q range and discuss the hierarchic structure of the shish-kebab.

2. Experimental Section

We used two kinds of polyethylene to prepare a blend. One is high molecular weight hydrogenated polyethylene (HMW-h-PE) with molecular weight M_w = 2 000 000 and polydispersity M_w/M_n = 12, and the other is low molecular weight deuterated PE (LMW-d-PE) with M_w = 200 000 and M_w/M_n = 5, where M_w and M_n are the weight- and number-average molecular weights, respectively. The nominal melting temperatures of HMW-h-PE and LMW-d-PE determined by DSC measurements were 135 and 132 °C at a heating rate of 20 °C/min. HMW-h-PE and LMW-d-PE were dissolved in xylene with antioxidant regent (2,6-*tert*-butyl-*p*-cresole) to form a homogeneous solution at 130 °C under a nitrogen atmosphere. The concentration of HMW-h-PE component was 2.8 wt %. After keeping the solution at 130 °C for 1 h, it was quenched into ice/water to precipitate as a gel, filtered from xylene, and washed with methanol several times. The gel was vacuum-dried at 70 °C for 2 days and then hot-pressed at 165 °C for 5 min and quenched rapidly to ice/water to obtain a film ~0.5 mm thick. Strips of the blend film were elongated about 6 times at a rate of 30 s^{-1} at 133 °C and quenched to ice/water. These elongated strips were aligned on the cell window.

Small-angle neutron scattering (SANS) measurements were performed using three spectrometers. One is the F-SANS spectrometer at JRR-3 reactor in Tokai with recently developed neutron focusing lenses made of MgF_2 with diameter 30 mm, curvature radius 25 mm, and thickness 10.5 mm. Using F-SANS, we can perform two-dimensional measurements in a very low Q ($= 4\pi \sin\theta/\lambda$, 2θ being the scattering angle) range from 1×10^{-4} to 10^{-2} Å^{-1}. We also used SANS-U[23] at JRR-3 reactor in Tokai. In the SANS-U measurements, the scattering vector Q was from 6×10^{-3} to 7×10^{-2} Å^{-1}. In addition, we used a time-of-flight (TOF) SANS spectrometer SWAN[24] installed at a spallation pulse cold neutron source at KENS, Tsukuba, in order to extend the Q range up to 3 Å^{-1}. In this spectrometer we measure the scattering intensity as a function of neutron wavelength λ as well as scattering angle $2q$. Hence, we can cover a very wide Q range from 10^{-2} to 3 Å^{-1} in the measurements. Combining all the data by three spectrometers, we can cover a Q range from $\sim 1 \times 10^{-4}$ to 3 Å^{-1} in this study. This wide Q range is a distinct feature of this experiment. The scattering data obtained in each spectrometer was corrected according to the standard procedure in the corresponding facility but not converted to the absolute intensity.

Small-angle and wide-angle X-ray scattering (SAXS and WAXS) measurements were performed using three spectrometers. WAXS measurements were carried out using a X-ray generator DX-GE-2P (JEOL) with a 2D imaging plate (IP) detector. The Q range covered in the WAXS measurement was 1.5×10^{-1}–3.1 Å^{-1}. SAXS measurements were carried out using an apparatus installed at the beamline BL45XU[25] in the SR facility, SPring-8, in Nishiharima. A CCD camera (C4880: Hamamatsu Photonics K.K.) with an image intensifier was used as a detector system for the SAXS measurements. In the measurement we covered a Q range of 4×10^{-3}–2×10^{-1} Å^{-1}. We also used U-SAXS machine with Bonse-Hart type camera (TRY-HV), which covered a Q range of 1×10^{-5}–8×10^{-3} Å^{-1}.

3. Results and Discussion

One of the aims in this work is to see the row structure (or the long oriented structure in micrometers) and the shish structure (or the extended chain crystal) in a wide Q range to determine the form factors. For this purpose we used hydrogen/deuterium (H/D) labeling method in SANS. We briefly explain the basic idea of the SANS measurements. We expect that the row structure and/or the shish structure is mainly formed from the HMW-h-PE in the blend.[17] It is well-known in SANS that the scattering contrast between hydrogenated and deuterated PEs is very large,[26] so that if the row structure and/or the shish structure is formed from HMW-h-PE we could observe them due to the high scattering contrast. On the other hand, in SAXS the scattering contrast arises from the electron density difference, which corresponds to the mass density difference in one-component systems. Therefore, in the case that the row structure and/or the shish structure are formed from HMW-h-PE, we expect very large difference between the SANS and SAXS profiles. However, if the HMW-h-PE chains are homogeneously distributed in the shish and the kebab structure, the SANS intensity in the small-angle region arises from the density fluctuations and the concentration fluctuations of HMW-h-PE in the shish and in the kebab. The former and latter are similar to those observed in the SAXS and to those in semidilute polymer solutions, respectively, and the latter are not so large compared with the former. Hence, in this case, we expect that the scattering patterns are almost identical in both the SANS and SAXS. Therefore, we can see whether or not the row structure and/or the shish structure is mainly formed from the HMW-h-PE by comparing the SANS data to the SAXS data. On the basis of this idea, we have performed SANS measurements on the blend of HMW-h-PE/LMW-d-PE (2.8/97.2). As shown in Figure 1, the streaklike scattering normal to the elongation direction is observed only in the SANS data. This result directly shows that the row structure and/or the shish structure is mainly formed from the HMW-h-PE although the Q range is not enough to estimate the form factor of the row structure. In order to evaluate the form factor, we have extended the Q range in this work.

Figure 2a shows the F-SANS data in a Q range down to 4×10^{-3} Å^{-1}, which shows anisotropic scattering pattern as expected from the SANS-U data (Figure 1a). After subtracting the background (the empty cell), the one-dimensional intensities have been calculated and plotted in Figure 3 in the parallel and normal directions, where the SANS-U data are also plotted in the parallel and normal directions. Figure 2b shows the 2D SWAN (TOF-SANS machine) data in low angle counters for neutron wavelength λ = 11 Å. Here we again observed the streaklike scattering in the direction normal to the elongation. One of the advantages in the SWAN measurements is to observe scattering intensities from crystalline lattices in the high Q range, which mainly come from the kebab structure.

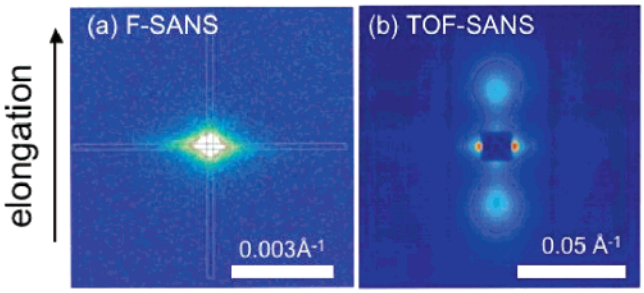

Figure 2. 2D SANS patterns of elongated PE blend of LMW-d-PE and HMW-h-PE: (a) measured by F-SANS and (b) measured by SWAN (TOF-SANS machine).

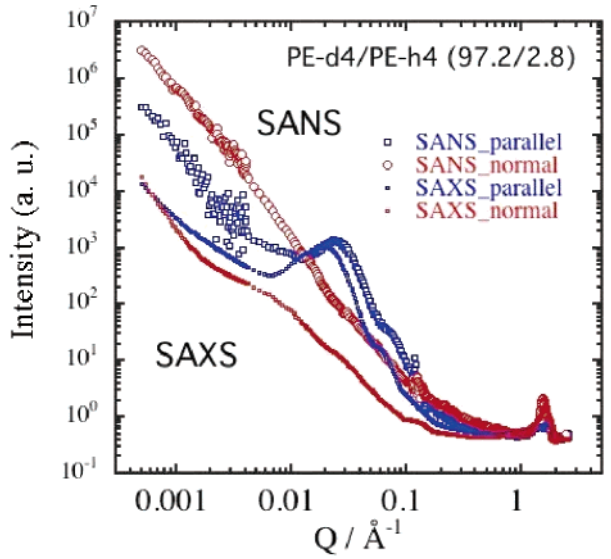

Figure 3. 1D SANS and SAXS profiles of elongated PE blend of LMW-d-and HMW-h-PE in the directions normal and parallel to the elongation direction.

In the large scattering angle region in SWAN, we observed a very strong Bragg intensity from the (110) plane in the normal direction, but the (200) diffraction is not so different between the normal and parallel directions, suggesting that the kebab grows along the *b*-axis although the data are not shown here. After correcting the data for the background (the empty cell) scattering, the counter efficiency, the wavelength distribution of incident neutron intensity, and the transmittance, we have calculated 1D scattering intensities in the parallel and normal directions and plotted in Figure 3. The data were shifted by eye so as the data are smoothly connected.

Data analysis is not straightforward in the measurements. As mentioned above, the SANS contrast in the present sample arises from two causes: the scattering length density difference due to the mass density difference and the scattering length difference between H and D. We assume that the mass density correlation function and the H/D density correlation function could be decoupled because the fraction of HMW-h-PE is very small (2.8 wt %). Furthermore, we assume that the row structure and/or the shish structure is formed from HMW-h-PE, and the other parts include only LMW-d-PE because the scattering contrast of the streaklike scattering in the SANS is very strong compared with the contrast in the SAXS (see Figures 1 and 2). Under the assumptions the scattering intensity could be approximated by

$$I(Q) = (\rho_{cD} - \rho_{aD})^2 I_{den}(Q) + (\rho_{cH} - \rho_{cD})^2 P_{row}(Q) \quad (1)$$

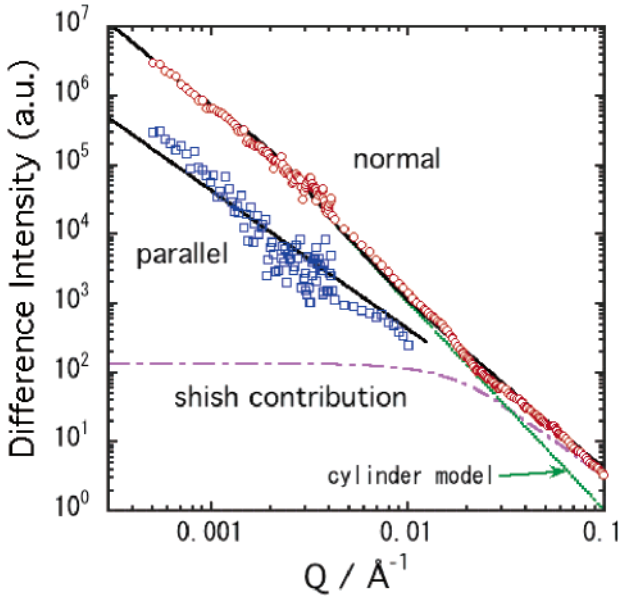

Figure 4. 1D SANS difference intensities in the directions normal and parallel to the elongation direction after subtraction of the contributions of density fluctuations which were evaluated from SAXS data. Thick solid lines (black) are the results of fit to multicore−shell cylinder model, and the chain line (purple) is a contribution of the core [or the shish (extended chain crystal)]. Thin solid line (green) is the result of fit to the cylinder model.

Here, ρ_{cD}, ρ_{aD}, and ρ_{cH} are the scattering length densities of d-PE in the crystalline region, d-PE in the amorphous region, and h-PE in the crystalline region, respectively, and $I_{den}(Q)$ and $P_{row}(Q)$ are the structure factor due to the mass density fluctuations and the form factor of the row structure (or the row structure including the shish). The former corresponds to Fourier transform of the mass density correlation function. In SAXS measurements h-PE and d-PE cannot be distinguished, and $I_{den}(Q)$ can be observed in SAXS with different scattering contrast, leading to eq 2.

$$I(Q) = KI_{den}(Q) + (\rho_{cH} - \rho_{cD})^2 P_{row}(Q) \quad (2)$$

where K is a ratio of contrast factor of neutron scattering to X-ray scattering.

In order to subtract the scattering contribution due to the mass density fluctuations $I_{den}(Q)$ in eq 2, we have carried out WAXS, SAXS, and U-SAXS measurements on the same sample and plotted in Figure 3 together with the neutron data. The X-ray intensity was adjusted so that the intensity ratio of WAXS to WANS is equal to the calculated one, and both of the intensities are the same at $Q = 0.4-0.6$ Å^{-1} because the structure fluctuations are very small at around $Q = 0.4-0.6$ Å^{-1}.[27] In the normal direction, the intensity difference between X-ray and neutron is very large, especially in a low Q range below about 0.1 Å^{-1}, confirming that the row structure and/or the shish structure is formed by the HMW-h-PE. On the other hand, in the parallel direction, the intensity difference is not very large, suggesting that the kebab is mainly formed from the LMW-d-PE although the small differences in the intensity and the peak position of the long period mean that the small amount of HMW-h-PE is included in the kebab. According to eq 2, we have subtracted the X-ray scattering intensity in both the directions, and the difference intensities are plotted in Figure 4. In this procedure we have neglected the incoherent scattering contribution mainly from hydrogen atoms in HMW-h-PE because it is very small in the measurement.

The difference intensities could be regarded as a form factor of the row structure (or the row structure including the shish) in both the parallel and perpendicular directions. However, the subtraction does not work well in the long period region ($0.01 < Q/\text{Å}^{-1} < 0.1$) in the parallel direction because the scattering contrast due to the density fluctuations in the kebab is very large and a small amount of h-PE is included in the kebab. Therefore, we did not use the data in the long period region ($0.01 < Q/\text{Å}^{-1} < 0.1$) in the parallel direction for further analyses to evaluate the form factors of the row structure and/or the shish structure.

In the low Q range between 3×10^{-3} and 2×10^{-2} Å^{-1} the scattering intensity in the normal direction can be described by a power law with an exponent of -3; $I(Q) \sim Q^{-3}$, corresponding to the asymptotic behavior of scattering intensity from a cylinder in the normal direction to the long axis, and hence we have first employed a cylinder model. The form factor of an oriented cylinder with a length of $2H$ and a radius of R has been reported by Shibayama et al.[28] According to the report, we have calculated the form factor in the normal direction taking into account the distributions of the radius R and the polar angle α of cylinder axis with respect to the elongation direction and fitted to the observed scattering intensity after convoluting with the resolution functions of the spectrometers. We found that the R distribution was not negligible but the angular distribution was very small, and hence the α distribution was neglected in the fits. The result of fit is shown by a thin line (green) in Figure 4, which is almost behind the data points (or a thick line) in the Q range below about 0.02 Å^{-1}. This means that the cylinder model can describe the row structure in the large scale above about 300 Å, and the evaluated radius was ~ 1 μm. This large radius certainly is not an extended chain crystal (shish) because it is large enough to include the kebab inside, but it is probably the bundle of the shish-kebab's. In the Q range above about 0.02 Å^{-1}, on the other hand, the observed data in the normal direction show excess scattering intensity, suggesting some extra structure which is not included in the cylinder model. As mentioned in the Introduction, Keller and co-workers[18−21] reported the shish structure with a diameter of $\sim$100 Å, which may correspond to an extended chain crystal (the shish). We have assigned the excess scattering intensity above about 0.02 Å^{-1} to the shish structure (the extended chain crystal). In order to describe this contribution, we employed a core−shell cylinder model,[29] in which the core and shell describe the extended chain crystal (the shish) and the row structure on the micrometer scale, respectively. The scattering intensity is given by

$$I_{\text{core-shell}}(Q) = [V_{\text{shell}}(\rho_{\text{shell}} - \bar{\rho}_{\text{D}})F(Q,R_{\text{shell}},H) + V_{\text{core}}(\rho_{\text{core}} - \rho_{\text{shell}})F(Q,R_{\text{core}},H)]^2 \quad (3)$$

where $F(Q,R,H)$ is scattering amplitude of a cylinder with a length of $2H$ and a radius of R, V_{shell}, V_{core}, R_{shell}, and R_{core} are the shell and core volumes and the shell and core radii, respectively, and ρ_{shell}, ρ_{core}, and $\bar{\rho}_{\text{D}}$ are the scattering length densities of the shell, the core, and the d-PE matrix, respectively. In this calculation we assumed $\rho_{\text{core}} = \rho_{\text{cH}}$, and $\bar{\rho}_{\text{D}}$ was calculated assuming that the shell volume fraction was 0.3 and HMW-h-PE was homogeneously distributed in the shell with the degree of crystallinity of 0.68 which were determined by the SAXS data. $\bar{\rho}_{\text{D}}$ was calculated under an assumption that the matrix consisted of only LMW-d-PE. According to eq 3, we calculated the scattering intensity of the core−shell cylinder model and fitted to the observed one in the normal direction. It was unfortunately found that the contribution of the core scattering in this model was too small to reproduce the observed intensity above about 0.02 Å^{-1}. Then we further assume that several extended chain crystals (the shishs) are included in the large shell cylinder. In the core−shell cylinder model the cross-term between the core and the shell is negligible small because of the small amount of HMW-h-PE. Hence, neglecting the cross-terms between core and core and between core and shell in this model, the scattering intensity could be approximated by

$$I_{\text{core-shell}}(Q) = [V_{\text{shell}}(\rho_{\text{shell}} - \bar{\rho}_{\text{D}})F(Q,R_{\text{shell}},H)]^2 + n[V_{\text{core}}(\rho_{\text{core}} - \rho_{\text{shell}})F(Q,R_{\text{core}},H)]^2 \quad (4)$$

where n is number of the core cylinders in a shell cylinder. The result of fit is shown by a thick solid line (black) in Figure 4 where the core (shish) contribution was also indicated by a chain line (purple). The result of fit is very good, showing that the present model, which is termed a multicore−shell cylinder model, is appropriate to describe the row structure and the shish structure. The evaluated radii of the shell and core are ~ 1 μm and 45 Å, respectively, and the number of the core cylinders is about 3, giving a picture that the row structure with radius of ~ 1 μm includes about three extended chain crystals (shish) with a diameter (a radius) of 90 Å (45 Å). This very small number of the shishs is one of the reasons why we did not observe the extended chain crystals in SAXS measurements. If we assume that the three shish-kebab structures equally share the large bundle (or the row structure) with radius of ~ 1 μm, the radius of the kebab would be about 5000 Å. We estimated the dispersions of the radius for the shell and the core, which were about $30 \pm 5\%$ and $\sim$5%, respectively. The latter is rather small, showing that the radius of the extended chain crystals is rather uniform.

We also calculated the form factor in the parallel direction, but it was impossible to fit to the observed data in the present Q range because the length of cylinder was too long. The ratio of scattering intensity in the parallel direction to the normal one is a function of the cylinder length in this Q range.[28] Hence, fixing all the geometrical parameters in the multicore−shell cylinder model except for the length, we calculated the intensity in the parallel direction and fitted to the observed data to reproduce the ratio of the intensity in the parallel direction to the normal one. The result is shown by a thick solid line (black) in Figure 4, and the estimated length of the cylinder $2H$ was ~ 12 μm. This length is comparable to that of the shish observed by Keller and co-workers by TEM.[18−21] The internal structure of the row structure is schematically drawn in Figure 5, where the size and amount of the kebabs are reduced and the noncrystalline short chains are not shown to clarify the internal structure.

In the previous experiments on crystallization of PE and isotactic polypropylene (iPP) after applying pulse shear,[16,17,22] we found that long oriented structure on the micrometer scale (which termed shishlike structure in the previous papers[16,17]) appeared in the very early stage of crystallization. Similar shishlike structure was reported in some papers and assigned to a precursor of the shish.[10−12,14] We also found that the formation of the shishlike structure (or the precursor) was enhanced by addition of high molecular weight component above a certain critical concentration, which was about 3 times larger than the overlap concentration of the high molecular weight component.[17] This result suggests that entanglements of high molecular weight components play an important role for the shishlike structure (or the precursor) formation. We therefore proposed a gel-spinning-like formation mechanism for the shishlike structure (or the precursor) in the previous paper,[17] in

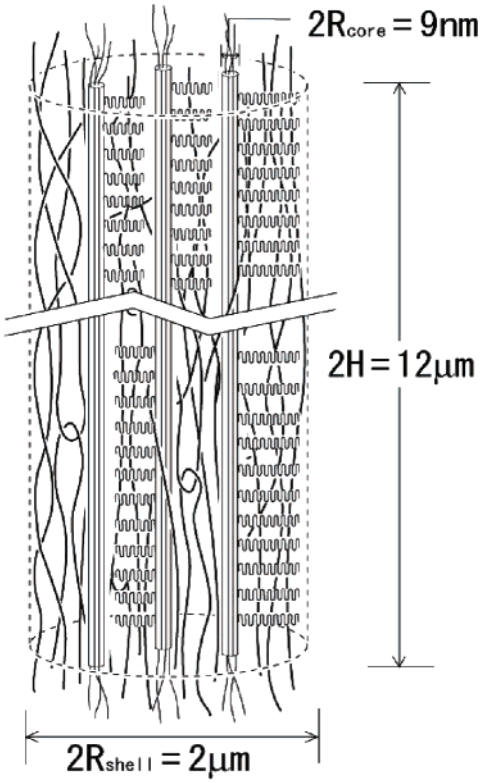

Figure 5. Schematic drawing of the row structure in micrometer scale including three shishs (extended chain crystals). The size ratio of R_{shell} (=1 μm) to R_{core} (=45 Å) is reduced very much to show both in the figure. Thick curves in the row structure represent the deformed oriented network of high molecular weight chains due to entanglements, and the noncrystallized short chains are not drawn here. The size and amount of the kebabs on the shish are reduced to show the internal structure.

which the long oriented shishlike structure is formed from deformation of network of high molecular weight chains due to entanglements. Recent experiment on isotactic polystyrene (iPS) showed that long oriented structure similar to the shishlike structure appeared on the micrometer scale after applying pulse shear even above the nominal melting temperature,[30] supporting the idea that the shishlike structure is formed from deformed oriented network of high molecular weight chains. It should be noted that the shishlike structure in the early stage of crystallization after applying pulse shear is very similar to the row structure in size observed in the elongated PE blend including small amount of HMW-h-PE although the crystallization mechanism after pulse shear may not be the same as that in the elongation process. The similarity in the structure suggests that the row structure in the elongated blend is also formed from the deformed oriented network of high molecular weight chains. The extended chain crystals may grow inside the row structure in micrometers although the mechanism is still unknown.

4. Conclusion

In this work we studied the hierarchic structure of shish-kebab of a blend of HMW-h-PE and LMW-d-PE in a wide spatial scale from angstroms to several micrometers using three SANS spectrometers and analyzed the data quantitatively on the basis of a multicore−shell cylinder model to determine the size parameters of the row structure and the shish structure (the extended chain crystal). It was found that the radii of the core and shell cylinders, which correspond to the shish and the row structure, were ∼45 Å and ∼1 μm, respectively, the length was ∼12 μm, and the number of the core cylinders in the large row structure was only 3. The results give a picture that the bundle of the shish-kebab structure (or the row structure) with a radius of ∼1 μm includes about three extended chain crystals (shishs) with a radius of ∼45 Å. This small number of the extended chain crystals is probably a reason why SAXS cannot detect the shish structure. We believe that the row structure is formed from the deformed oriented network of high molecular weight chains due to entanglements, in which the extended chain crystals may grow.

Acknowledgment. We are grateful to Professor Shibayama and Dr. Fujisawa for the support in SANS measurements with SANS-U and SAXS measurements at BL45XU, respectively.

References and Notes

(1) Keller, A.; Kolnaar, J. W. H. In *Processing of Polymers*; Meijer, H. E. H., Ed.; VCH: New York, 1997; pp 189−268.
(2) Samon, J. M.; Schultz, J. M.; Hsiao, B. S.; Seifert, S.; Stribeck, N.; Gurke, I.; Collins, G.; Saw, C. *Macromolecules* **1999**, *32*, 8121−8132.
(3) Kumaraswamy, G.; Issaian, A. M.; Kornfield, J. A. *Macromolecules* **1999**, *32*, 7537−7547.
(4) Pogodina, N. V.; Siddiquee, S. K.; Egmond, J. W. v.; Winter, H. H. *Macromolecules* **1999**, *32*, 1167−1174.
(5) Somani, R. H.; Hsiao, B. S.; Nogales, A.; Srinivas, S.; Tsuo, A. H.; Sics, I.; Balta-Calleja, J.; Ezquerra, T. A. *Macromolecules* **2000**, *33*, 9385−9394.
(6) Kumaraswamy, G.; Verma, R. K.; Issaian, A. M.; Wang, P.; Kornfield, J. A.; Yeh, F.; Hsiao, B.; Olley, R. H. *Polymer* **2000**, *41*, 8934−8940.
(7) Nogales, A.; Somani, R. H.; Hsiao, B. S.; Srinivas, S.; Tsuo, A. H.; Balta-Calleja, J.; Ezquerra, T. A. *Polymer* **2001**, *42*, 5247−5256.
(8) Pogodina, N. V.; Lavrenko, V. P.; Srinivas, S.; Winter, H. H. *Polymer* **2001**, *42*, 9031−9043.
(9) Kumaraswamy, G.; Kornfield, J. A.; Yeh, F.; Hsiao, B. *Macromolecules* **2002**, *35*, 1762−1769.
(10) Somani, R. H.; Yang, L.; Hsiao, B. S. *Physica A* **2002**, *304*, 145−157.
(11) Somani, R. H.; Young, L.; Hsiao, B. H.; Agarwal, P. K.; Fruitwala, H. A.; Tsuo, A. H. *Macromolecules* **2002**, *35*, 9096−9104.
(12) Seki, M.; Thurman, D. W.; Oberhauser, J. P.; Kornfield, J. *Macromolecules* **2002**, *35*, 2583−2594.
(13) Elmoumni, A.; Winter, H. H.; Waddon, A. J.; Fruitwala, H. *Macromolecules* **2003**, *36*, 6453−6461.
(14) Yang, L.; Somani, R. H.; Sics, I.; Hsiao, B. H.; Kolb, R.; Fruitwala, H.; Ong, C. *Macromolecules* **2004**, *37*, 4845−4859.
(15) Hsiao, B.; Yang, L.; Somami, R. H.; Avila-Orta, C. A.; Zhu, L. *Phys. Rev. Lett.* **2005**, *94*, 117802-1−118902-4.
(16) Fukushima, H.; Ogino, Y.; Matsuba, G.; Nishida, K.; Kanaya, T. *Polymer* **2005**, *46*, 1878−1885.
(17) Ogino, Y.; Fukushima, H.; Matsuba, G.; Takahashi, N.; Nishida, K.; Kanaya, T. *Polymer* **2006**, *47*, 5669−5677.
(18) Odell, J. A.; Grubb, D. T.; Keller, A. *Polymer* **1978**, *19*, 617−626.
(19) Bashir, Z.; Odell, J. A.; Keller, A. *J. Mater. Sci.* **1984**, *19*, 3713−3725.
(20) Bashir, Z.; Odell, J. A.; Keller, A. *J. Mater. Sci.* **1986**, *21*, 3993−4002.
(21) Bashir, Z.; Hill, M. J.; Keller, A. *J. Mater. Sci., Lett.* **1986**, *5*, 876−878.
(22) Ogino, Y.; Fukushima, H.; Takahashi, N.; Matsuba, G.; Nishida, K.; Kanaya, T. *Macromolecules* **2006**, *39*, *7617*−7625.
(23) Ito, Y.; Imai, M.; Takahashi, S. *Physica B* **1995**, *213/214*, 889−891.
(24) Otomo, T.; Furusaka, M.; Satoh, S.; Itoh, S.; Adachi, T.; Shimizu, S.; Takeda, M. *J. Phys. Chem. Solids* **1999**, *60*, 1579−1582.
(25) Fujisawa, T.; Inoue, K.; Oka, T.; Iwamoto, H.; Uruga, T.; Kumasaka, T.; Inoko, Y.; Yagi, N.; Yamamoto, M.; Ueki, T. *J. Appl. Crystallogr.* **2000**, *33*, 797−800.
(26) Bacon, G. E. *Neutron Diffraction*; Clarendon Press: Oxford, 1975.
(27) Wiegand, W.; Ruland, W. *Prog. Colloid Polym. Sci.* **1979**, *66*, 355−366.
(28) Shibayama, H.; Nomura, S.; Hashimoto, T.; Thomas, E. L. *J. Appl. Phys.* **1989**, *66*, 4188−4197.
(29) Nakano, M.; Matsuoka, H.; Yamaoka, H.; Poppe, A.; Richter, D. *Macromolecules* **1999**, *32*, 697−703.
(30) Kanaya, T.; Takayama, Y.; Ogino, Y.; Matsuba, G.; Nishida, K. In *Progress of Understanding of Polymer Crystallization*, *Lecture Notes in Physics*; Reiter, G., Strobl, G., Eds.; Springer: Berlin, 2006; pp 91−99.

MA062606Z